Electromechanical transducer for rapid detection, discrimination and quantification of lung cancer cells

2016 Nanotechnology 27 195101

(http://iopscience.iop.org/0957-4484/27/19/195101)

IOP Publishing Nanotechnology
Nanotechnology 27 (2016) 195101 (10pp) doi:10.1088/0957-4484/27/19/195101

Electromechanical transducer for rapid detection, discrimination and quantification of lung cancer cells

Waqas Ali[1,2,3], Fatemeh Jalvhei Moghaddam[4], Muhammad Usman Raza[1,2,3], Loan Bui[4], Bailey Sayles[4], Young-Tae Kim[4,5] and Samir M Iqbal[1,2,3,4,5]

[1] Nano-Bio Lab, University of Texas at Arlington, Arlington, Texas 76019, USA
[2] Department of Electrical Engineering, University of Texas at Arlington, Arlington, Texas 76019, USA
[3] Nanotechnology Research Center, University of Texas at Arlington, Arlington, Texas 76019, USA
[4] Department of Bioengineering, University of Texas at Arlington, Arlington, Texas 76010, USA
[5] Department of Urology, University of Texas Southwestern Medical Center at Dallas, Dallas, TX 75235, USA

E-mail: SMIQBAL@uta.edu

Received 7 December 2015, revised 15 February 2016
Accepted for publication 16 February 2016
Published 29 March 2016

Abstract

Tumor cells are malignant derivatives of normal cells. There are characteristic differences in the mechanophysical properties of normal and tumor cells, and these differences stem from the changes that occur in the cell cytoskeleton during cancer progression. There is a need for viable whole blood processing techniques for rapid and reliable tumor cell detection that do not require tagging. Micropore biosensors have previously been used to differentiate tumor cells from normal cells and we have used a micropore-based electromechanical transducer to differentiate one type of tumor cells from the other types. This device generated electrical signals that were characteristic of the cell properties. Three non-small cell lung cancer (NSCLC) cell lines, NCI-H1155, A549 and NCI-H460, were successfully differentiated. NCI-H1155, due to their comparatively smaller size, were found to be the quickest in translocating through the micropore. Their translocation through a 15 μm micropore caused electrical pulses with an average translocation time of 101 $\pm$ 9.4 μs and an average peak amplitude of 3.71 $\pm$ 0.42 μA, whereas translocation of A549 and NCI-H460 caused pulses with average translocation times of 126 $\pm$ 17.9 μs and 148 $\pm$ 13.7 μs and average peak amplitudes of 4.58 $\pm$ 0.61 μA and 5.27 $\pm$ 0.66 μA, respectively. This transformation of the differences in cell properties into differences in the electrical profiles (i.e. the differences in peak amplitudes and translocation times) with this electromechanical transducer is a quantitative way to differentiate these lung cancer cells. The solid-state micropore device processed whole biological samples without any pre-processing requirements and is thus ideal for point-of-care applications.

Keywords: lung cancer, cell cytoskeleton, cell mechanics, electromechanical transducer, thin film membrane, cancer diagnosis, point-of-care

(Some figures may appear in colour only in the online journal)

1. Introduction

The efficacy of cancer treatments largely depends on the extent to which the tumor spreads [1, 2]. Detecting the tumor in the early stages makes treatment much easier and also elevates the chances of recovery [3–5]. There are various transformations that happen at the molecular and cellular levels before a cancer matures and appears at the tissue and

organ levels [2, 3]. It has been reported that the cytoskeletons of cells characteristically alter during cancer transformations [6–9]. The cytoskeleton of a cell is a complex polymer network that defines the molecular architecture of cells and is involved in many cellular functions. It evolves during the differentiation of cells [10, 11]. The mechanical properties and morphologies of cells depend on the cytoskeleton, and thus, any change in the cytoskeleton affects the mechanical properties of the cells. The mechanical properties of individual living cells are closely related to the health and function of the human body [3, 6, 12]. Cancer inception and progression can be related to changes in the cell cytoskeleton. Continuous monitoring and tracking of cell cytoskeleton modifications can give a better understanding of this disease and can make timely detection possible. During cancer progression, the cytoskeleton transforms to a more compliant and irregular state from an ordered and rigid structure [7, 12, 13]. This restructuring of the cytoskeleton makes malignant cells more motile and pliable compared with normal cells and also helps them to replicate themselves more quickly [14, 15]. Owing to these well known facts, cell elasticity, rigidity, size, shape irregularity and lower resistance to deformation (i.e. softness) have emerged as new biological cell markers to differentiate tumor cells from normal cells and also to distinguish between types of tumor cells (e.g. metastatic versus non-metastatic) [15–17].

Micropipette aspiration (MA), microneedle probes, atomic force microscopy (AFM), microplate manipulation and optical tweezers, among other techniques, have previously been used to investigate cell mechanical properties [18–22]. Lekka *et al* probed the mechanical properties of normal and cancerous cells with AFM and found an order of magnitude difference in cell rigidity [14]. Ward *et al* have reported a 50% difference in the elasticity of malignant and normal cells using MA. All of these methods have their limitations [13, 23], requiring labor-intensive pre-processing of the samples, specialized equipment and very well trained manpower to get the results. The results can't be obtained quickly. Probing the cell cytoskeleton directly requires fluorescent tagging [7]. There are no convenient methods to investigate mechanical properties of cells and to differentiate them on that basis. To address these challenges, an electromechanical transduction approach has been previously reported to analyse a mixed population of normal and cancer cells that simulated a biopsy sample [17, 30, 33]. Those works discriminated cancer cells from white/red blood cells and also showed that bladder cancer cells could be clearly separated from the normal urothelial cells using micropore biosensors. The micropore approach is capable of transforming these mechanical properties of individual cells into electrical signals. The micropore transducer generates unique electrical pulses for each cell type based on the mechanical properties of the individual cells. Distinct electrical pulses are obtained for cells with different physical and mechanical properties (elasticity, motility, shape, size, malignancy etc), whereas similar electrical pulses are seen for cells with the same properties.

A micropore electromechanical transducer is a resistive-pulse sensor. The ionic current through the micropore changes as the cells pass through it under a mechanical force. Smaller and more elastic and motile cells can squeeze through the micropore easily and quickly whereas cells with less elasticity, motility and larger size face more resistance to their passage, and as a result spend more time in the micropore and are characterized by slow translocation. Narrow and shallower electrical pulses mark fast translocation, whereas deeper and wider pulses are characteristic of slower translocation.

A major challenge post-diagnosis is the selection of the right treatment, i.e. once tumor cells have been differentiated from the normal cells, how can it be rapidly and objectively ascertained if the tumor is an adenocarcinoma or a squamous carcinoma. Another major question would be to determine whether the cells are from a metastatic or non-metastatic tumor. This work focuses on these challenges, as about 85%–90% of lung cancers are NSCLCs [24]. There are three subtypes of NSCLC cells: squamous cell (epidermoid) carcinoma, adenocarcinoma and large cell (undifferentiated) carcinoma [24–26]. About 25%–30% of all lung cancers are squamous cell carcinomas, 40% are adenocarcinomas and about 10%–15% are large cell carcinomas [24]. The cells of these subtypes differ in size, shape and chemical make-up when observed optically. Experiments with micropore translocation differentiated NSCLC cell lines A549, NCI-H460 and NCI-H1155. NCI-H1155 and NCI-H460 are large cell lung cancer subtypes and A549 is an adenocarcinoma subtype of NSCLC [25]. The device successfully enumerated more than 75% of cells for each cell type and generated unique electrical profiles for each of these based on their unique mechanophysical properties.

2. Materials and methods

2.1. Micropore device fabrication

The micropore membrane that is the backbone of the device is fabricated using microelectromechanical systems (MEMS) fabrication techniques. A double-side polished (DSP), silicon wafer of (100) crystallographic orientation is used to create the device. The DSP wafer is first cleaned in a piranha solution (H_2SO_4:H_2O_2 at 1:1) and then oxidized in a oxygen environment in a three-zone furnace at 1100 °C. Exposing the wafer to such an ambient environment yields a 1 μm thick oxide layer on both sides of the wafer. A reflectometer is used to determine the exact thickness of the oxide layer.

After this, the wafer is prepared for photolithography by first cleaning it in the piranha solution for 10 min. Then the wafer is dried using dry nitrogen and dehydrated on a hot plate at 150 °C. Shipley 1813 positive photoresist is spin-coated on both sides of the DSP wafer, which is then processed under UV light with a dark field mask that transfers the pattern of the etch windows on to the wafer. Then an MF319 developer is used to develop the transferred pattern. Buffered hydrofluoric acid (BHF) is used to etch away the oxide and transfer the square window patterns in the oxide and reveal

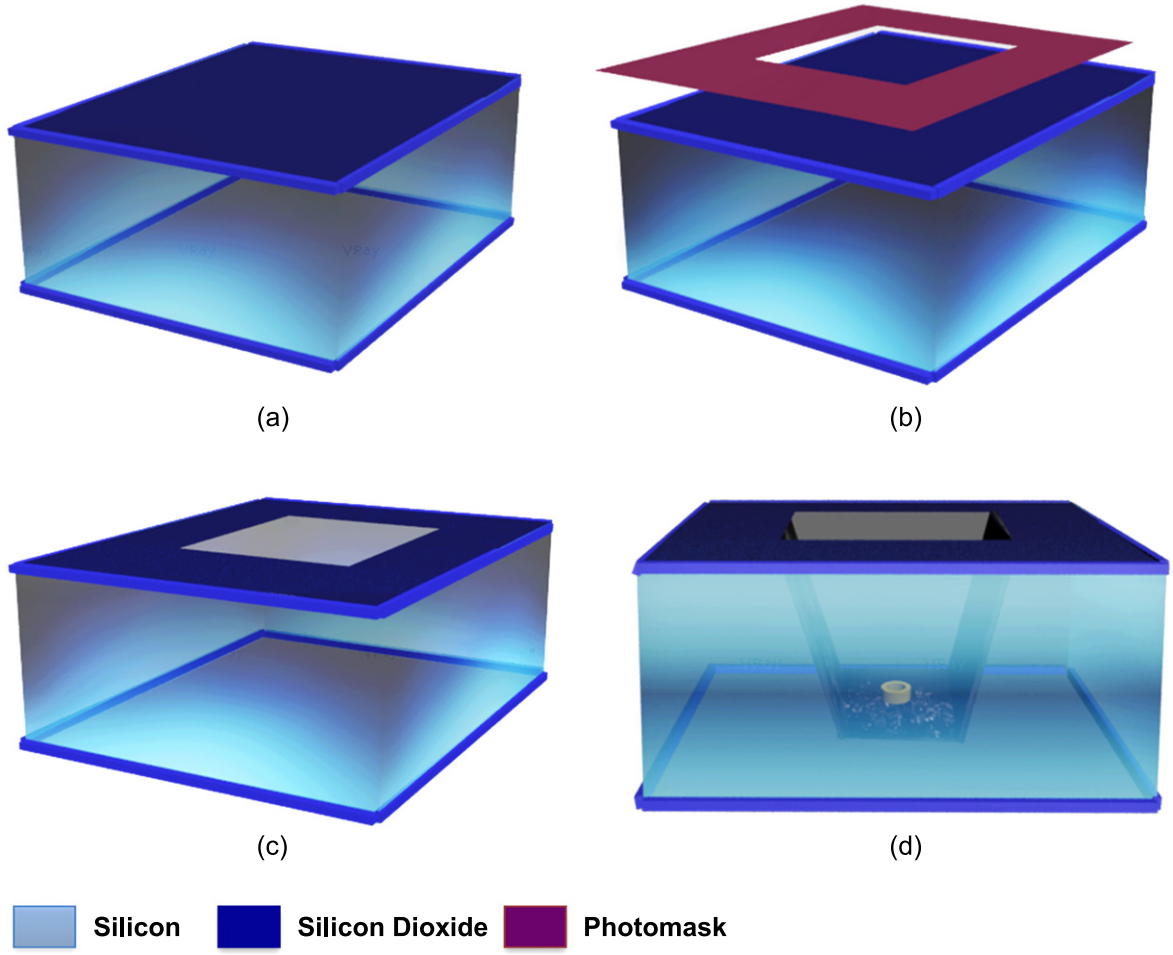

Figure 1. Micropore device fabrication steps. (a) A DSP silicon wafer is oxidized and (b) one side of the wafer is patterned with optical photolithography to (c) open square etch windows. (d) Silicon is etched through these windows with TMAH to make thin suspended silicon dioxide membranes.

the bare silicon underneath. After this, acetone is used to remove the remaining resist from both sides of the wafer.

The wafer is then immersed in a 25% tetramethylammonium hydroxide (TMAH) solution at 90 °C with steady stirring at 200 rpm. TMAH is an anisotropic etchant of silicon and etches with high selectivity into the (100) face of the silicon at a rate of about 1 μm min^{-1} [27]. As the wafer is 525 μm thick it takes about 10 h for the etching of the (100) layer to reach the back side and reveal the 1 μm thick SiO_2 membranes on the other side of the wafer. The fabrication steps are shown in detail in figure 1.

The wafer is then cut into 5 × 5 mm^2 individual chips, each of which has an SiO_2 membrane. The chips are then processed under a focused ion beam (FIB) to drill the free-standing SiO_2 membrane, which creates a single micropore of about 15 μm in diameter in each chip. An acceleration voltage of 30 kV and beam current of 1 nA are used for 200 s to fabricate the 15 μm diameter micropore. By varying the exposure time, beam current and acceleration voltage, micropores of 1–50 μm can be fabricated [17, 28–30]. After drilling, each chip is annealed at a high temperature for a few seconds to smoothen the walls of the micropore and to relieve stresses in the oxide membranes that could cause cracking during the experiments [28].

2.2. Measurement setup

The micropore chip was sandwiched between polydimethylsiloxane (PDMS) gaskets, which were further sandwiched between two Teflon blocks. The Teflon blocks contained the buffer solution (0.85 wt% NaCl). The assembly ensured that during the experiments the only translocation path was through the micropore, and the solution did not leak through or around the assembly. The PDMS gaskets and the Teflon blocks had 1 mm holes. The micropore chips were placed inside the gaskets in such a way that all of the holes in the Teflon blocks and gaskets were aligned with the micropore membrane (figure 2).

Voltage bias and ionic current recordings were done through an Ag/AgCl electrode pair. One electrode was dipped in each reservoir and these were connected to the data acquisition cards in a computer. After this, the cells were pumped into the inlet reservoir using a syringe pump. When a cell passed through the micropore, it physically blocked the

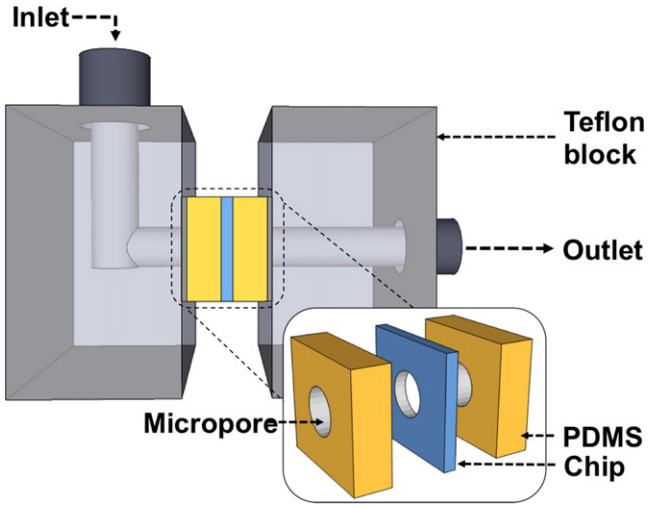

Figure 2. Experimental setup for cancer cell discrimination. A $5 \times 5\,mm^2$ micropore chip is sandwiched between PDMS gaskets, which are further sandwiched between two Teflon blocks. The Teflon blocks contain the electrolyte solution and cells are inserted into one of the blocks (i.e. the inlet) with a syringe pump.

micropore for a certain period of time, leading to a change in the conductivity of the micropore. This conductivity is measured by the relation $G = \sigma\pi r^2/L$, where σ is the conductivity of the NaCl solution, r is the micropore radius and L is the channel length/membrane thickness. When the cell physically blocked the micropore, its effective radius was reduced; leading to a reduction in the ionic current passing though the micropore. The data acquisition cards relayed the information to a LabView program that was used to collect and store the experimental data. The acquired data was analysed with MATLAB routines [31].

2.3. Lung cancer cell line cultures

The three NSCLC cell lines (A549, NCI-H460 and NCI-H1155) were obtained from the University of Texas Southwestern Medical Center at Dallas in Texas, USA. These cells were maintained as per the standard approved protocols. The cells were cultured in an RPMI-1640 medium with 10% heat-inactivated fetal bovine serum. Gentamycin and L-glutamine (Invitrogen) were also added to the cell culture medium. The cells were cultured under a sterile, humidified, 95% air:5% CO_2 environment at 37 °C.

2.4. Measurement of lung cancer cell diameter

The three lung cancer cell lines were dissociated with Trypsin-EDTA (0.05%) and seeded on a hemocytometer to measure the cell diameters. The dissociated cancer cells were imaged ($n = 30$ for each cell line) and their diameters were measured by *ImageJ* software. For statistical analysis, the averages and the standard deviations were calculated and ANOVA was carried out.

2.5. Lung cancer cell migration through tightly confined microchannels

To investigate the mechanical and elastic differences among the three different lung cancer cell types, cell migration via tightly confined microchannels was quantified. The lung cancer cells were separately seeded (10 000 cells per device, $n = 20$ for each cell type) in the microchannel device described in [32]. The microchannel device had two reservoirs, one to seed the cells and another to receive them through tapered microchannels. The microchannels were 5 μm high and 530 μm long. Their widths gradually decreased from 20 μm to 15, 10, 8 and finally to 5 μm just before the receiving reservoir (figures 3(c)–(e)). All devices were coated with Collagen type 1 overnight at 37 °C. The microchannel devices were incubated at 37 °C and 5% CO_2, and the cells were allowed to migrate through microchannels for 7 days. After 7 days, the cells were fixed with 4% paraformaldehyde in 1× phosphate-buffered saline (PBS) and stained with 4′,6-diamidino-2-phenylindole (DAPI). The cells that had migrated from the microchannels into the receiving reservoirs were then counted with a fluorescent microscope. For statistical analysis, the average and the standard deviation were calculated and a *t*-test was carried out.

3. Results

3.1. Cell detection efficiency

For each lung cancer cell line, a sample with a known concentration was translocated through the micropore chip. The process was repeated twice. Each cell registered one pulse when it translocated. The efficiency of cell registration was calculated from the recorded pulses as:

$$\text{Cell detection efficiency } (\eta) = \frac{\text{No. of single cell pulses detected}}{\text{Total number of cells introduced}} \times 100$$

The detection efficiency η for each cell type was greater than ~75% for a flow rate of 1 ml h^{-1} and a 0.2 MHz sampling frequency. Cell detection efficiency is a strong function of the sampling frequency and cell flow rate. This combination of flow rate and sampling frequency was chosen after a series of experiments as this gave highest detection efficiency. Using a very high flow rate deteriorated device selectivity. On the other hand, if the flow rate was too low or if the sampling frequency was too high or too low then the device lost sensitivity [33]. Trade-offs between the device sensitivity, selectivity and throughput are essential to decide the flow rate and sampling frequency.

High detection efficiency is a much needed property for this technology. During the initial stages of cancer, the number of tumor cells is extremely low in the lesion [25, 34, 35]. If the device is not sensitive enough, the detection efficiency will be low resulting in false negatives. A detection efficiency of 75% indicates that 25% of the cells

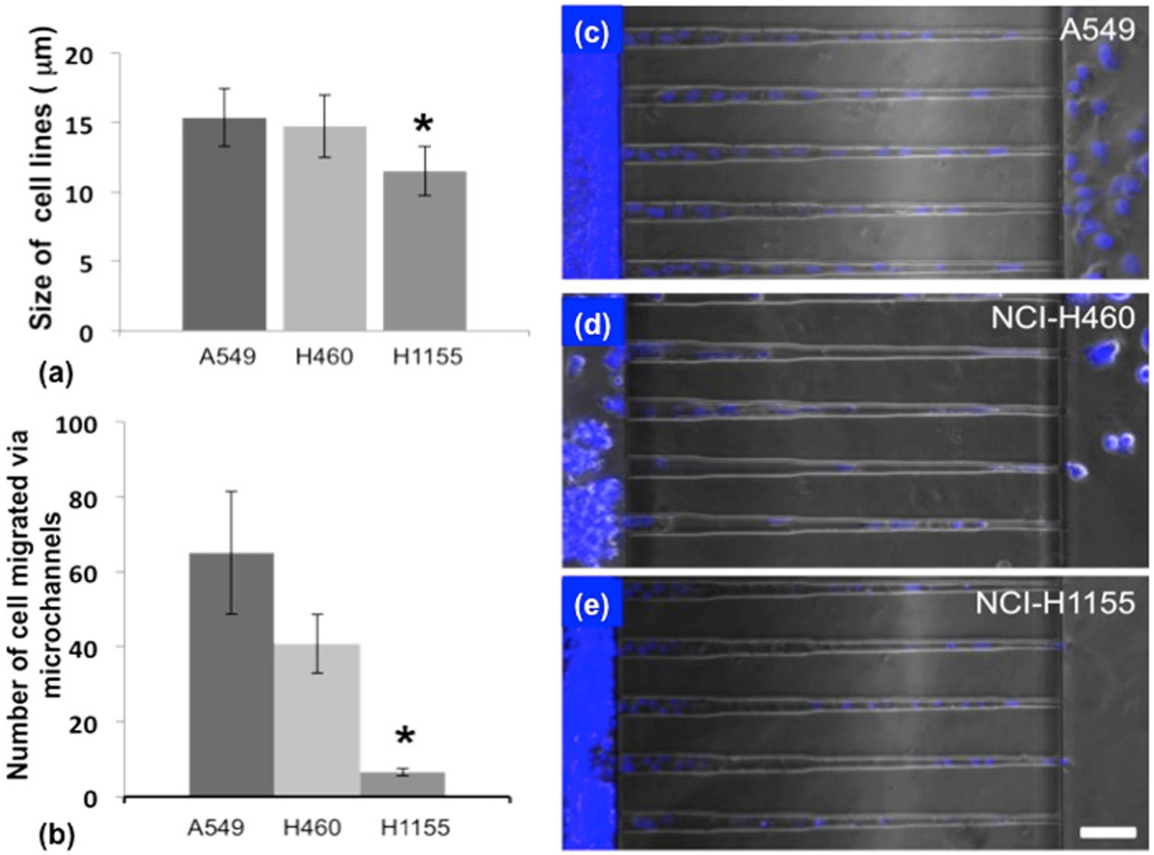

Figure 3. Quantitative comparison of cell size and migration ability. (a) The cell diameter was measured from the optical images of cells ($n = 30$) of each tumor type and average cell size was calculated. The average cell sizes of A549 and NCI-H460 were found to be very similar, whereas NCI-H1155 was found to be much smaller in size. Average $\pm$ s.d. $*p < 0.01$ between NCI-H1155 and others. (b) Number of cells migrated from the seeding reservoir to the receiving reservoir via tapered microchannels. Average $\pm$ S.E.M. $*p < 0.05$ between NCI-H1155 and others. $n = 20$/each cell line. Representative micrographs of (c) A549, (d) NCI-H460 and (e) NCI-H1155 traveling through microchannels. Scale bar $= 50\ \mu$m. Migration experiments were repeated three times.

were either clumped together or were too small for registration. Pulses with multiple spikes were from cell clumps and were discarded during the analysis. This caused a reduction in the cell detection efficiency. The device was thus sensitive enough to register all pulses for almost all of the cells that translocated through the micropore. Cell clumping is also a property of metastatic cells. A single spike thus indicated the presence of a single cell inside the micropore and multiple spikes showed that there were multiple cells traversing the micropore simultaneously [17].

About one clogging event occurred for roughly every ten experiments. This required the device to be disassembled and the micropore washed. Cell clumps were also observed, and these were the major cause of reductions in the device detection efficiency. To solve these issues, i.e. cell clustering and pore clogging, chemical agents could be used to break the epithelial cellular adhesion molecule (EpCAM). This would break clumps into single cells and would avoid any cell clustering or pore clogging, but would add a sample pre-processing step to the protocol. However, even without this additional sample pre-processing, a cell detection efficiency of ~75% was achieved.

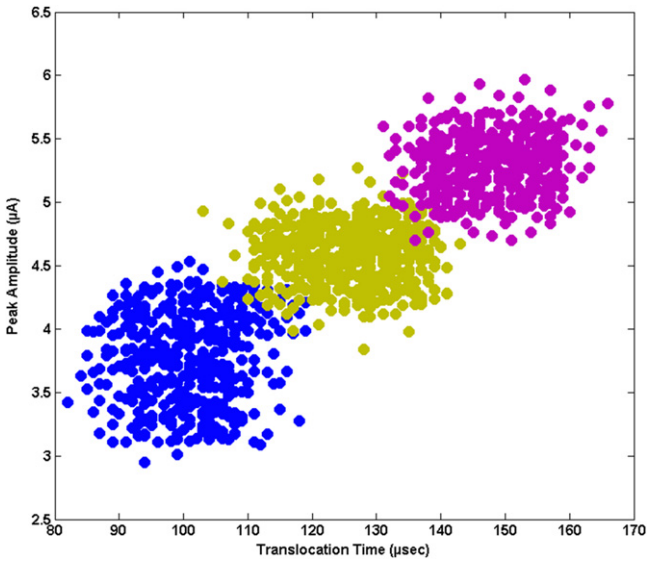

Figure 4. Scatter plot for NCI-H1155 (blue), A549 (yellow) and NCI- H460 (purple). Data points for all three NSCLC cell lines are plotted together for comparison. The density populations for NCI-H1155, A549 and NCI-H460 are confined in separate regions, indicating that the electrical pulses associated with them have different peak amplitude and pulse width characteristics.

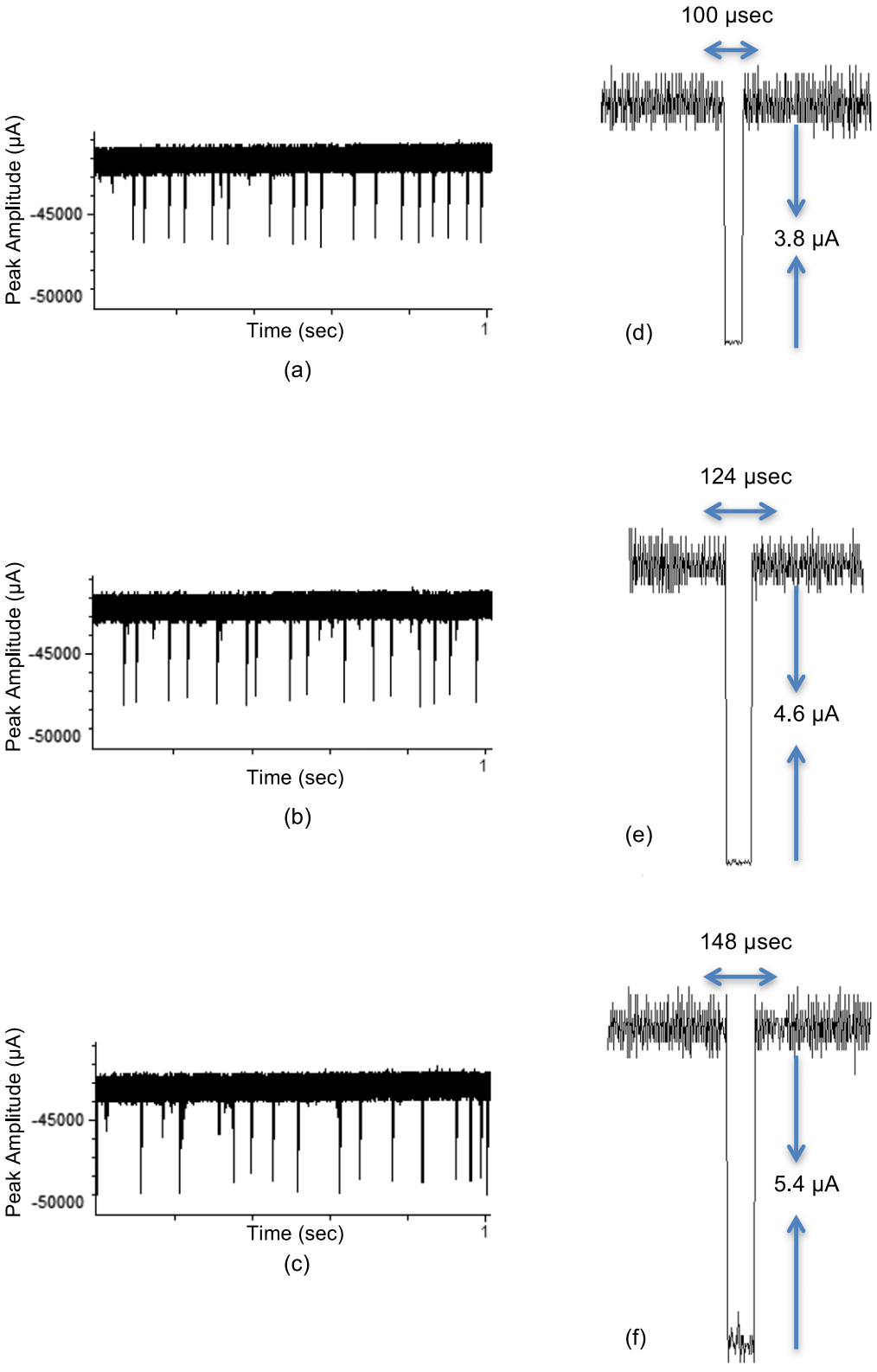

Figure 5. Signature pulses of the three cancer cell types. (a)–(c) The ionic current through a 15 μm micropore showing representative pulses from the translocation of (a) NCI-H1155, (b) A549 and (c) NCI-H460 for a 1 s duration. Zoomed-in views of representative pulses for NCI-H1155, A549 and NCI-H460 are shown in (d), (e) and (f), respectively.

Table 1. Pulse statistics for NSCLC cells through micropore.

Cell Line	Average translocation time (μs)	Average peak amplitude (μA)
NCI-H1155	101 ± 9.4[a]	3.71 ± 0.42[b]
A549	126 ± 17.9[a]	4.58 ± 0.61[b]
NCI-H460	148 ± 13.7[a]	5.27 ± 0.66[b]

[a] $P < 0.0001$, $n = 1500$.
[b] $P < 0.0001$, $n = 1500$.

3.2. Electrical signatures of the lung cancer cells

The cancer cells were suspended in an NaCl buffer solution at a concentration of 1000 cells ml^{-1}. Each vial was thoroughly shaken to suspend the cells homogenously in the buffer. The three cell suspensions were then pumped through the micropore, one by one, with the aid of a syringe pump for 40–60 min. While translocating through the micropore, each type of cell caused significant blockage to the ionic current flow and that reduction in ionic current was recorded as dips in the baseline current of the micropore.

After data acquisition for all three NSCLC cell lines, the recorded pulses were analysed. First, the pulse statistics (pulse width and amplitude values) were extracted using a MATLAB routine and then statistical analysis of the data was done by an ANOVA test. The test confirmed that there were three different populations of data. Each data cluster was associated with a particular cell type. These populations are plotted in figure 4. Each cell type shows a unique cluster that is different from the cluster recorded for the other two cell lines. The signature pulses of each cell type are shown in figure 5. The unique characteristics of the electrical pulses were their peak amplitudes and pulse widths (table 1). Pulses registered for NCI-H1155 had an average peak amplitude of 3.71 μA (s.d. 0.42) and an average pulse width of 101 μs (s.d. 9.4), for A549 the average peak amplitude was 4.58 μA (s.d. 0.61) and the average pulse width was 126 μs (s.d. 17.9) and for NCI-H460 the average peak amplitude and the average pulse width were 5.27 μA (s.d. 0.66) and 148 μs (s.d. 13.7), respectively.

3.3. Cell quantification from a mixed lung cancer cell suspension

After identifying the electronic signatures of each lung cancer cell type, two separate mixtures were prepared and processed through the micropore one by one. In the first mixture, 5000 cells of each cell type were suspended in 10 ml NaCl solution (total 15 000 cells). In the second mixture, different numbers of cells of each cell type were suspended in 10 ml NaCl. This mixture contained 1000 cells of NCI-H1155, 5000 cells of A549 and 10 000 cells of NCI-H460. So the final mixture had a total of 16 000 cells in 10 ml of solution with NCI-H1155, A549 and NCI-H460 in a 1:5:10 ratio. Each mixture was processed through a 15 μm micropore for 40–60 min.

For each suspension the cell detection efficiency was >∼75%. The registered pulses associated with a particular cell line were counted to determine the number of cells of that cell line present in each mixture. The pulse count obtained from the acquired data was found to be close to the known numbers of the introduced cells in the suspension for each cell type. The registered pulses for mixtures 1 (1:1:1) and 2 (1:5:10) are shown in figures 6(a) and (b) respectively, for a period of 1 s. Three different types of pulses can be readily identified in these representative samples. For the mixed suspension with equal concentrations of three lung cancer cell types, the representative sample of 1 s contained 8 pulses that had the features of NCI-H1155 and 6 pulses each with the features of A549 and NCI-H460 (figure 6(a)). The representative sample for the mixed suspension of unequal concentrations (1:5:10) shows 2 pulses with the features of NCI-H1155, 6 pulses with the characteristics of A549 and 13 pulses with NCI-H460 features (figure 6(b)).

The scatter plots in figures 6(c) and (d) show the density populations of the pulses obtained from the translocation of mixture 1 and mixture 2, respectively. In both plots there are three distinct populations that indicate the presence of three different types of cells in each mixture. In the first scatter plot (figure 6(c)) the three distinct populations have similar densities, which confirms that the three types of cells present in the mixture have same concentration, whereas the second scatter plot (figure 6(d)) shows that the three types of cells present in the mixture are not at the same concentrations, as expected in figure 6(c), the left lower data points belong to NCI-H1144, the center cluster depict A549 cells and the right top data indicate NIH-H460 cells. These experiments clearly show that the different types of NSCLC cells present in a sample were detected, as well as quantified, with this technology. This differentiation stemmed from their unique mechanophysical properties.

The average cell diameters of A549 and NCI-H460 are about the same, whereas NCI-H1155 is significantly smaller (figure 3(a)). To elucidate the elastic-deformability properties of these cells that resulted in the translocation differences, another set of experiments was done with tapered microchannels. The microchannels provided gradually reducing constrictions to the migration of cells. Significantly higher numbers of A549 and NCI-H460 cells completely migrated to the receiving reservoir via the tightly confined microchannels as compared to NCI-H1155 (figures 3(b)–(e)). Higher numbers of A549 cells migrated via the microchannels as compared to NCI-H460 cells, but there was no statistical difference between them. All three cell lines migrated toward the opening of the microchannels (20 × 5 μm^2), but NCI-H1155 cells could not migrate via the ending of the tapered microchannels (5 × 5 μm^2), despite these were smaller in diameter.

4. Discussion

To differentiate one type of tumor cell from another using micropore technology, it is necessary that both types of cells are different in their physical, mechanical and molecular properties. This difference is inherent in tumor cells as the cell cytoskeleton is affected during cancer and as a result the cell

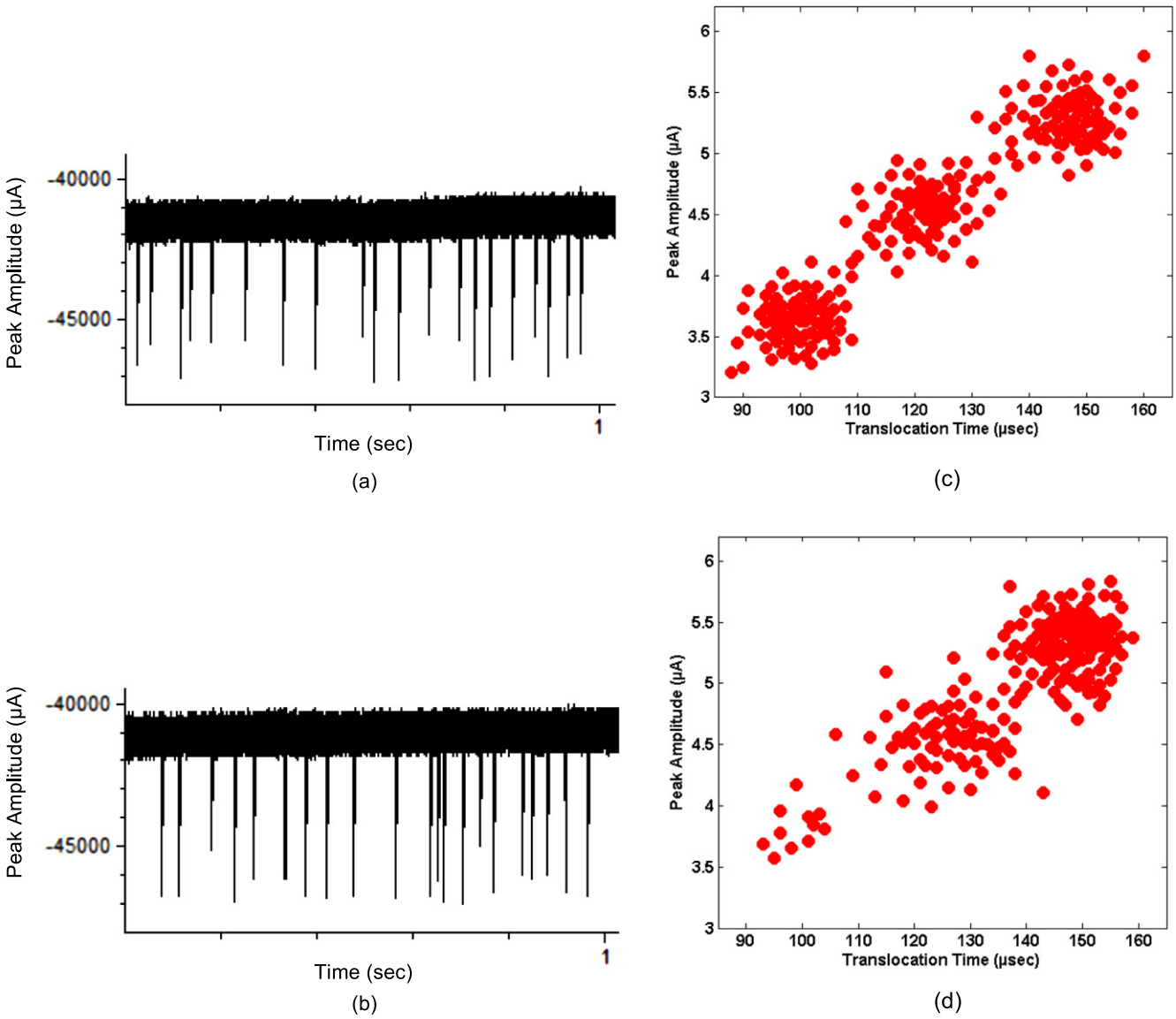

Figure 6. Signature pulses and scatter plots of mixed suspensions of three lung cancer cell lines. The ionic current through a 15 μm micropore showing pulses from the translocation of cell suspensions containing NCI-H1155, A549 and NCI-H460 at ratio of (a) 1:1:1 and (b) 1:5:10 for 1 s duration and their respective scatter plots in (c), (d). The ratio of the number of pulses from each cell line closely represents the ratio of the number of cells present in each mixture.

properties are modified [3, 7, 20, 36, 37]. Depending on the stage and type of cancer, the transformations are much more evident, ultimately leading to clear differences in the cell attributes. As micropore electromechanical transduction is highly sensitive to these differences and hence quantifiably differentiates tumor cells, this technique can be used to determine the stage and type of a cancer, which are very important in cancer diagnosis and treatment [5, 38].

The three subtypes of NSCLC are different from each other in their cell attributes [24, 39]. Although A549 and NCI-H460 have almost the same cell size, as shown in figure 3, they differ in other cell characteristics such as elasticity and flexibility. On the other hand, small-sized NCI-H1155 cells faced much less steric hindrance from the micropore walls [33], and were able to translocate easily through the micropore. Between A549 and NCI-H460, the longer translocation time and higher peak amplitude of the pulses for the latter indicate that it is less deformable and dynamic compared to A549, and this is exactly what we observed from the cell migration behavior of both types of tumor cells through the tapered microchannels (figure 3). Many more A549 cells migrated from one side of the microchannel to the other side than NCI-H460 cells. This directly supports the strength of the micropore approach for cancer-sensing capability. Among the three tumor cell types, the smallest number of NCI-H1155 cells were able to migrate from one side of the tapered microchannel to the other. The fast translocation of NCI-H1155 cells from the micropore device and their cell migration behavior through the tapered microchannel at first seem to be contradictory results, but this is not the case as among the three cell types NCI-H1155 is the smallest in size. Owing to this, despite being less dynamic

and elastic, as seen in the tapered channel migration experiment, they were able to translocate through the micropore easily and quickly. So size is the dominant factor and a prime contributor to the translocation profile through the micropore, and cell elasticity, flexibility, cell shape and motility, etc only become important when the cell size is same for the translocating species.

A very important point to note here is that the cells must interact with the micropore walls to be discriminated on the basis of elasticity and flexibility. That is why this device had a pore size close to the size of A549 and NCI-H460. For discrimination between smaller cells, smaller micropores would be needed. The system cannot discriminate between cells that do not have to deform or squeeze through in order to pass through the pore. This device cannot discriminate between cell types that have different elasticities and flexibilities but are of the same size unless the pore size is comparable to the cell size. Keeping the micropore size comparable to the cell size is key to discriminating cells based on their elasticity/flexibility.

5. Conclusions

This electromechanical approach to detect and quantify NSCLC cells in a sample from a cancer patient using a micropore device is simple yet very efficient. Discriminating different types of tumor cells is a major step in disease diagnosis and treatment. The micropore approach can translate the differences in tumor cell properties into differences in electrical signals that can easily be interpreted. A patient's sample can be analysed with this device without any pre-processing requirements and without the need for fluorescent tagging or particle/bead attachment. The required results can be obtained within few hours, making it a suitable choice for point-of-care diagnostic applications.

Acknowledgments

We are thankful to Dr Robert Bachoo at UT Southwestern Medical Center for providing the lung cancer cells for experiments. We would also like to thank Dr M Arif I Mahmood for useful discussions and Mr Raja Raheel Khanzada and Mr Mohammad Raziul Hasan for help with imaging and graphics. This work was supported by the NSF grant ECCS-1201878 and CPRIT grant RP110041.

References

[1] Lennon A M *et al* 2014 The early detection of pancreatic cancer: what will it take to diagnose and treat curable pancreatic neoplasia? *Cancer Res.* **74** 3381–9
[2] Carter H B *et al* 2013 Early detection of prostate cancer: AUA guideline *J. Urol.* **190** 419–26
[3] Chaffer C L and Weinberg R A 2011 A perspective on cancer cell metastasis *Science* **331** 1559–64
[4] Gao Y and Yuan Z 2014 Nanotechnology for the detection and kill of circulating tumor cells *Nanoscale Res. Lett.* **9** 500
[5] Marino N, Woditschka S, Reed L T, Nakayama J, Mayer M, Wetzel M and Steeg P S 2013 Breast cancer metastasis: issues for the personalization of its prevention and treatment *Am. J. Pathol.* **183** 1084–95
[6] Fife C M, McCarroll J A and Kavallaris M 2014 Movers and shakers: cell cytoskeleton in cancer metastasis *Br. J. Pharmacol.* **171** 5507–23
[7] Lukinavicius G *et al* 2014 Fluorogenic probes for live-cell imaging of the cytoskeleton *Nat. Methods* **11** 731–3
[8] Ohnishi Y, Watanabe M, Yasui H and Kakudo K 2014 Effects of epidermal growth factor on the invasive activity and cytoskeleton of oral squamous cell carcinoma cell lines *Oncol. Lett.* **7** 1439–42
[9] Pritchard R H, Huang Y Y and Terentjev E M 2014 Mechanics of biological networks: from the cell cytoskeleton to connective tissue *Soft Matter* **10** 1864–84
[10] Agus D B *et al* 2013 A physical sciences network characterization of non-tumorigenic and metastatic cells *Sci. Rep.* **3** 1449
[11] Wang Y *et al* 2014 DLC1-dependent parathyroid hormone-like hormone inhibition suppresses breast cancer bone metastasis *J. Clinic. Invest.* **124** 1646–59
[12] Chambers A F, Groom A C and MacDonald I C 2002 Dissemination and growth of cancer cells in metastatic sites *Nat. Rev. Cancer* **2** 563–72
[13] Ward K A, Li W I, Zimmer S and Davis T 1991 Viscoelastic properties of transformed cells: role in tumor cell progression and metastasis formation *Biorheology* **28** 301–13
[14] Lekka M, Laidler P, Gil D, Lekki J, Stachura Z and Hrynkiewicz A 1999 Elasticity of normal and cancerous human bladder cells studied by scanning force microscopy *Eur. Biophys. J. Biophys. Lett.* **28** 312–6
[15] Suresh S 2007 Nanomedicine: elastic clues in cancer detection *Nat. Nanotechnol.* **2** 748–9
[16] Lee G Y and Lim C T 2007 Biomechanics approaches to studying human diseases *Trends Biotechnol.* **25** 111–8
[17] Ilyas A, Asghar W, Ahmed S, Lotan Y, Hsieh J-T, Kim Y-t and Iqbal S M 2014 Electrophysiological analysis of biopsy samples using elasticity as an inherent cell marker for cancer detection *Anal. Methods* **6** 7166–74
[18] Benitez R and Toca-Herrera J L 2014 Looking at cell mechanics with atomic force microscopy: experiment and theory *Microsc. Res. Tech.* **77** 947–58
[19] De la Rica R, Thompson S, Baldi A, Fernandez-Sanchez C, Drain C M and Matsui H 2009 Label-free cancer cell detection with impedimetric transducers *Anal. Chem.* **81** 10167–71
[20] Dehoux T, Abi Ghanem M, Zouani O F, Ducousso M, Chigarev N, Rossignol C, Tsapis N, Durrieu M C and Audoin B 2014 Probing single-cell mechanics with picosecond ultrasonics *Ultrasonics* **56** 160–71
[21] Kuznetsova T G, Starodubtseva M N, Yegorenkov N I, Chizhik S A and Zhdanov R I 2007 Atomic force microscopy probing of cell elasticity *Micron* **38** 824–33
[22] Li Q S, Lee G Y H, Ong C N and Lim C T 2008 AFM indentation study of breast cancer cells *Biochem. Biophys. Res. Commun.* **374** 609–13
[23] Guo Y-J, Sun G-M, Zhang L, Tang Y-J, Luo J-J and Yang P-H 2014 Multifunctional optical probe based on gold nanorods for detection and identification of cancer cells *Sensors Actuators* B **191** 741–9
[24] McGuire M J *et al* 2014 Identification and characterization of a suite of tumor targeting peptides for non-small cell lung cancer *Sci. Rep.* **4** 4480
[25] Han Y, Su C and Liu Z 2014 Methods for detection of circulating cells in non-small cell lung cancer *Front. Biosci.* **19** 896–903
[26] Minamimoto R *et al* 2014 A pilot study of 4′-[methyl-11C]-thiothymidine PET/CT for detection of regional lymph node metastasis in non-small cell lung cancer *EJNMMI Res.* **4** 10

[27] Tabata O, Asahi R, Funabshi H, Shimaoka K and Sugiyama S 1992 Aanisotropic etching of silicon in TMAH solutions *Sensors Actuators* A **34** 51–7
[28] Asghar W, Ilyas A, Billo J A and Iqbal S M 2011 Shrinking of solid-state nanopores by direct thermal heating *Nanoscale Res. Lett.* **6** 372–7
[29] Asghar W, Ilyas A, Deshmukh R R, Sumitsawan S, Timmons R B and Iqbal S M 2011 Pulsed plasma polymerization for controlling shrinkage and surface composition of nanopores *Nanotechnology* **22** 285304
[30] Ilyas A, Asghar W, Kim Y T and Iqbal S M 2014 Parallel recognition of cancer cells using an addressable array of solid-state micropores *Biosens. Bioelectron.* **62** 343–9
[31] Billo J A, Asghar W and Iqbal S M 2011 An implementation for the detection and analysis of negative peaks in an applied current signal across a silicon nanopore *Proc. SPIE* **8031** 80312T
[32] Wan Y, Tamuly D, Allen P B, Kim Y-T, Bachoo R, Ellington A D and Iqbal S M 2013 Proliferation and migration of tumor cells in tapered channels *Biomed. Microdev.* **15** 635–43
[33] Asghar W, Wan Y, Ilyas A, Bachoo R, Kim Y T and Iqbal S M 2012 Electrical fingerprinting, 3D profiling and detection of tumor cells with solid-state micropores *Lab on a Chip* **12** 2345–52
[34] Breitenbuecher F *et al* 2014 Development of a highly sensitive and specific method for detection of circulating tumor cells harboring somatic mutations in non-small-cell lung cancer patients *PLoS One* **9** e85350
[35] Jemal A, Siegel R, Ward E, Hao Y, Xu J, Murray T and Thun M J 2008 Cancer statistics, 2008 *CA-A Cancer J. Clinic.* **58** 71–96
[36] Cross S E, Jin Y S, Rao J and Gimzewski J K 2007 Nanomechanical analysis of cells from cancer patients *Nat. Nanotechnol.* **2** 780–3
[37] Moeendarbary E and Harris A R 2014 Cell mechanics: principles, practices, and prospects *WIREs Syst. Biol. Med.* **6** 371–88
[38] Hofman V *et al* 2014 Detection of circulating tumor cells from lung cancer patients in the era of targeted therapy: promises, drawbacks and pitfalls *Curr. Mol. Med.* **14** 440–56
[39] Shoemaker R H 2006 The NCI60 human tumour cell line anticancer drug screen *Nat. Rev. Cancer* **6** 813–23